MANSOURA JOURNAL OF CHEMISTRY
Official Journal of Faculty of Science, Mansoura University, Egypt
E-mail: scimag@mans.edu.eg ISSN: 1687-5060

Highly Efficient Solar Driven Steam Generation via Derived Biomass Wastes

Omnia A. Allam, Doaa A. Kospa, Rania M. Eltabey, Amr Awad Ibrahim

Chemistry Department, Faculty of science, Mansoura University)
**** Correspondence to:** amr_awad@mans. edu.eg, Tel: 01091313272)*

Received:13/2/2023
Accepted:14/3/2023

Abstract: Solar desalination is a promising technique to remedy the worldwide water crisis with minimum environmental impact. Herein, we successfully converted the wood wastes (sawdust) to construct biochar as an evaporator. Plasmonic metal doped the biochar to enhance steam generation (SG) *via* the multiple nucleation sites, benefiting from their excellent light absorption. As a result, the evaporator achieves an evaporation rate of 0.657 kg m^{-2} h^{-1} (77.0% efficiency) under 1 sun illumination. The evaporator showed extraordinarily salt-resistant performance under 1 sun illumination to the different interactions of salt ions with the functional groups of biochar. Based on its facile and cost-effective fabrication process, excellent energy-conversion efficiency, salt-resistance, and durability, the prepared evaporator may be a promising generator for freshwater on a large scale.

keywords: Biochar, solar steam generation, water treatment.

1.Introduction

Water covers three-quarters of the earth's surface so considered one of the most abundant natural resources; however, only about 3% is potable. More than 80 countries suffer severe water shortages, and about 25% of the world's population does not have the appropriate quality or quantity of freshwater[1]. Besides, more than two-thirds of the world's population may encounter freshwater shortage by 2025 according to the World Watch Institute; hence, the problem is affecting every country in the world, including the developed, unless they provide additional water sources and reduce their demand [1]. Desalination is one of the most promising solutions to provide new freshwater in regard to the rapidly growing global water shortage. Reverse osmosis, capacitive deionization, multi-stage flash distillation, desalination batteries and Electro-dialysis are different technologies of desalination that were used in practice [2]. Although oceans and seas contain nearly 97% of the world's water, desalination only accounts for a small fraction of the world's potable water supply today because existing commercial techniques for desalination face important drawbacks such as large energy footprints and high capital costs [3]. Therefore, desalination can only become a sustainable freshwater source if new technologies are developed dramatically. Innovative desalination methods that reduce energy consumption and costs are constantly needed. Like the solar evaporation method, which uses the sun's free and abundant energy to create fresh water from polluted water, brackish water, and saltwater [4].

The most abundant natural renewable resource, solar energy can be used in a variety of processes, including photovoltaics [4], photocatalysis [5,6], and solar steam generation [4, 5]. The solar steam generation (SSG) technique uses a natural source of energy to refine water and is considered a strategy that is both technically viable and highly advantageous [6, 7]. However, this technique has low efficiency because of the significant environmental heat loss and the bulk water. Recently a bi-layered structure is used to improve efficiency by minimizing the dissemination of the transferred heat to the surrounding liquid. [8]. The bi-layered structure has a top layer that functions as high-efficiency photothermal conversion materials, ultra-broadband solar energy absorbers and a bottom layer that serves as an insulator to prevent heat from dissipating into bulk phase [9, 10]. Gauze [11], polyurethane foam (PU) [9], wood [7] and solid polystyrene

foam (PS) [10] have recently been employed as insulators in the development of SSG devices with high evaporation rates. Photothermal materials have ideal properties which contain porous networks, broadband absorbance of sunlight, good hydrophilicity, long-term stability and low loss of thermal energy As a result; they are regarded as critical components of the interfacial steam generating system [9, 10 Many types of evaporators, including plasmonic nanometals, (e.g., Au, Ag, Al)[5, 9], ceramic-based materials[10], semiconductor materials [11, 12], biomass-based materials [13], polymer-based materials [14, 15] and derived carbon materials [16, 17] have been found in recent years for SSG performance. However, the majority of the found materials are either costly or have extensive production procedures.

Because of their availability, low cost, environmental friendliness, and biological structure Recently, materials for solar steam generation from biomass have risen to the top of the list of favored evaporators [18]. Two main methods have been used to generate steam using BSSG materials. The first method, which is practical for the production of freshwater, uses biomass-derived materials in their original, undisturbed form[13]. However, because of their poor light-to-heat conversion efficiency, the majority of these materials vaporize slowly. The second method involves modifying the surface properties of plasmonic metals through, polymer deposition, plasmolysis, decoration or carbonization to increase the materials' capacity to absorb sunlight. [23]. the most common cellulosic biomass material is wood, which has mesoporous, hierarchical, and low-tortuosity structures. Due to its many characteristics, including its natural hydrophilicity, good mechanical properties, low thermal conductivity, high solar light absorption and countless aligned microchannels for quick water transport, harmless nature in water, and greater strength, Wood has lately generated a lot of scientific attention in the SSG process [19, 20]. However, a lot of biochar is created as a byproduct of the forest products industry and is either disposed of in landfills or used as boiler fuel. It may be more cost-effective to convert these residues into carbon-based material today than to dispose of them, as this is one of the most efficient evaporators.

A carbon-based substance called biochar is created when biomass wastes are carbonized in the presence of noble gases [21]. Due to its high permeability, advanced special surface area, large carbon percentage (65–92%), cost-effectiveness, simple manufacturing, and high carbon content in comparison to other conventional carbon-based materials, sawdust-derived biochar has a high potential for use in solar desalination. [22]. For SSG performance Low-temperature pyrolysis is favored to maintain the wood structure's numerous aligned microchannels, which improve water transport to the condenser interface, salt rejecting capability and light diffraction through the condenser by allowing the salt to redissolve back into the water [23]. On the other hand, copper nanoparticles (CuNPs) are the favored material for solar desalination because they are easily manufactured at a low cost and have excellent plasmonic characteristics in the visible-light spectrum.

Herein, a developed photothermal absorber was prepared by a simple and cost-effective fabrication method. The biomass wastes (sawdust) were collected and carbonized to porous biochar. The derived biochar was doped by copper nanoparticles. The fabricated absorbers (Cu/biochar) exhibited a high evaporation rate of 0.8 Kg m^{-2} h^{-1} with a heat-conversion efficiency of 80%. Moreover, the membrane yields high freshwater production under the real sun and from all types of contaminated seawater.

2. Materials and methods

2.1. Materials and chemicals

We acquired wood sawdust from an Egyptian furniture maker in Mansoura. Copper Acetate ($Cu(OAc)_2$. $2H_2O$), L-ascorbic acid (L-AA) and calcium chloride ($CaCl_2$) were obtained from Alfa Aeser. Sodium chloride (NaCl) and potassium chloride (KCl) were supplied from Merk.

2.2. Preparation of photo absorbers

2.2.1. Synthesis of biochar

First, a wood crusher was used to mill and chop the collected sawdust into pieces that were 3-4 mm in size. the powdered wood was

cleaned multiple times with DI water and ethanol to get rid of the contaminants before being heated for ten hours at 80 °C. The dried sample was heated in a vacuum oven for two hours at 350 °C, and the resulting sawdust was then ground to a powder.

2.2.2. Preparation of metal plasmonic

First, 20 ml of distilled water with 1 g of sawdust was ultrasonically mixed for 30 minutes. The Cu/biochar dispersion was then given 63 mg of copper acetate. H_2O, which was added and stirred for 15 minutes. Then, 126 mg of L- ascorbic acid as a reductant agent was dispersed in 25 mL of distilled water while the reaction mixture was vigorously stirred at 80 °C for an hour. The addition of NH_4OH solution maintained the solution's pH level at 10. Finally, the finished product (Cu/biochar) was separated, washed multiple times with distilled water, and then dried at 80 °C.

2.3. Material Characterization

Multiple analysis techniques were used to confirm the successful preparation. Using EDX methods and scanning electron microscopy (SEM, JEOL JSM 6510lv), the interfacial properties of the materials and their crystalline phase were examined. Moreover, X-ray photoelectron spectroscopy (XPS) with Thermo Fisher Scientific ESCALAB 250 was used in identifying and quantifying all surface elements. With a solar simulator (SciSun-300 AAA, a 300W xenon lamp, 5050 mm, and an AM 1.5G filter) and a power meter set to 1 kW/m2, the SSG performance was tested. UV-vis spectrophotometer and inductively coupled plasma-optical emission spectrometry (ICP-OES) were used to evaluate the amounts of metal ions and dyes before and after SSG experiments, respectively. The surface temperatures of each absorber were recorded using an infrared thermal camera (htti-xintai, IR-camera) and a thermocouple, respectively, during the desalination procedure. The X-ray diffraction peaks (XRD) of all condensers at 2θ (4^o-70^o) were determined using a Bruker system employing monochromated Cu-K radiation (=1.5418 Å), with initial values and scan step time of 0.02 and 0.80 s, respectively.

2.4. Manufacturing of a bi-layer SSG device

A top surface that indicates a photothermal absorber and a bottom layer that provides an insulator make up the system of the SSG bilayer. A piece of PU foam was drilled with pores that were 7 cm in diameter and 2 cm thick, and these holes were then covered with rolling cotton to transport water to the surface to prepare the bottom layer. In addition, a slurry was created by dissolving 50 mg of absorbers in 5 mL of distilled water for fifteen minutes The membrane was then vacuum-dried at 80 °C overnight after the suspension was placed into 7 cm of air-laid paper. As soon as possible, the membrane was attached to the bottom layer, and the system was then suspended in distilled or saline water.

2.5. Solar steam generation

60 minutes were spent using a solar simulator with a power meter set at 1 kW/m^2 with humidity of 22 °C and 50% and ambient temperatures, respectively. The mass loss was measured every five minutes during the SSG experiments with an automated electronic balance that had a 0.1 mg precision.

Equation (1) was used to calculate the evaporation rate (v).

Eq.1:

$$V = \frac{dm}{sdt} \quad (1)$$

Where ***m*** *(kg),* ***t*** *(h),* ***S*** *(m^2)* and ***v*** *(kg m^{-2} h^{-1})* are the mass change of water, time of light illumination, the cross-sectional area of the evaporator and evaporation rate, respectively.

Furthermore, equation (2) was used to calculate the energy efficiency (***η***).

Eq.2:

$$\eta = \frac{He\, v}{\mathrm{Qin}} \quad (2)$$

Where, ***He, η (energy efficiency),*** ***Qin***, are the sensitive heat of the whole liquid-vapor phase-change and the solar simulator's power density (1 kW/m^2), respectively, and ***He*** is calculated as follows:

Eq.3:

$$He = C\Delta T + \Delta h \quad (3)$$

Where and *Δh (2394 kJ/ kg), C* (4.18 j g^{-1} k^{-1}), *ΔT* (K) are enthalpy of water vaporization, the specific heat of water capacity and the change of water temperature, respectively.

3. Results and Discussion

3.1. Characterization of Materials

The results of utilizing the FT-IR spectrum to highlight the various functional groups in the structures of Cu and biochar are displayed in Figure 1a. Because of the lower pyrolysis temperature, biochar displayed a distinctive absorption band at 3365 cm^{-1} that corresponded to alcoholic and phenolic hydroxyl groups. The spectrum also revealed a clear peak at 1022 cm^{-1} that attributed to the carbohydrates (C-O) group. In addition, mineral peaks that are common to different wood (biochar) were found at 1590, 1720, and 2920 cm^{-1}, respectively, which correspond to the stretching aliphatic C-H vibrations, carboxyl group (C=O), and C=O and aromatic C=C stretching. Besides their low intensity, the distinctive peaks of the Cu/biochar composite's FTIR were those of biochar, showing that the plasmonic metal and biochar effectively coated each other [28, 29].

Additionally, using the XRD patterns was shown in Fig1b. It was possible to measure the crystallinity of each produced evaporator. Four similar reflections that are assumed to reflect features of cellulose structure were discovered in the SDB spectra. These peaks, which were measured at 2°; 15°, 17.4°, 22°, and 36°, were assigned the miller indices 101, 101', 002, and 040, respectively [24]. The Cu/biochar spectra revealed the characteristic CuNP peaks at 2= 43.5°, 50.5°, and 73.9° that correspond to (111), (200), and (220) planes and have crystallite diameters of approximately 16 nm [25]. Furthermore, the elimination of Cu_2O in the final particles proved that they were pure metallic Cu particles at 2= 35° and 41.5° [26].

SEM was used to examine the morphologies of the biochar and Cu/biochar specimen, and the resulting images are displayed in Fig. The biochar has a high porosity with twenty m micropores and oriented honeycomb-like groups of the surface pores according to these images. Additionally, it featured long cylindrical channels that offered suitable water capillarity paths [27, 28]. CuNPs were satisfactorily distributed on the biochar interface without harming the high porosity, according to SEM images (Fig. 2)

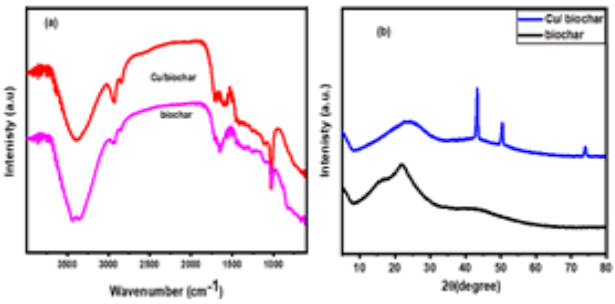

Fig. 1: (a) FT-IR spectra of biochar and Cu/biochar, (b) XRD pattern of biochar and Cu/biochar

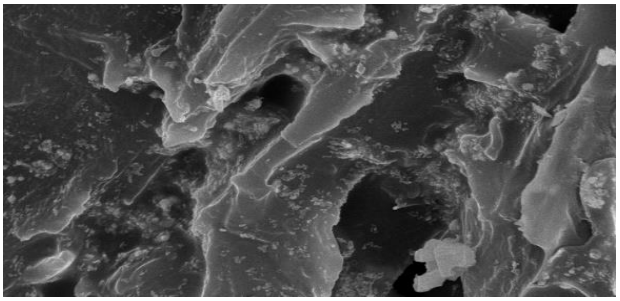

Fig. 2: SEM images of biochar and Cu/biochar

3.2. The (Cu/biochar) evaporator's performance in terms of steam production and thermal localization

Five 5 cm diameter thermal absorber membranes were made as follows: (filter paper, biochar, 5, 10, and 20% Cu/biochar) to evaluate the effectiveness of various prepared photothermal absorbers in producing steam. We compared the efficiency of all samples in producing solar steam when using pure filter paper under one sun's elimination for 60 minutes.

We comprised the solar steam generation effectiveness of all samples with pure filter paper under solar elimination of 1 sun over 1 hour by a xenon lamp. The evaporation rates of (filter paper, biochar, 5, 10, and 20% Cu/biochar) absorber are 0.326, 0.5636, 0.7195, and 0.774 kg m^{-2} h^{-1}, respectively. According to the low thermal absorption of PU foam and filter paper, the results indicated that pure filter paper has the lowest weight loss. Besides that, the incorporation of biochar by the plasmonic metal increased the evaporation rate, and the Cu/biochar membrane generated the greatest evaporation rate of 0.56 kg m^{-2} h^{-1}. The figure3a showed that the increase in the amount of copper nanoparticles loaded led to an increase in the evaporation rate which achieved 0.77 kg m^{-2} h^{-1}. Additionally, the solar evaporation efficiencies of all evaporators were

shown in Fig. 3b. The equation (2) is used to calculate the evaporation efficiencies of the various solar absorbers under one sun illumination, the evaporation efficiencies were calculated to be 32.2, 43.2, 55.7, 71.3 and 77%, respectively. According to these findings, the 20% Cu/biochar composite has a higher thermal efficiency than filter paper with a similar intensity and this result is exactly equivalent to that of recently published evaporators.

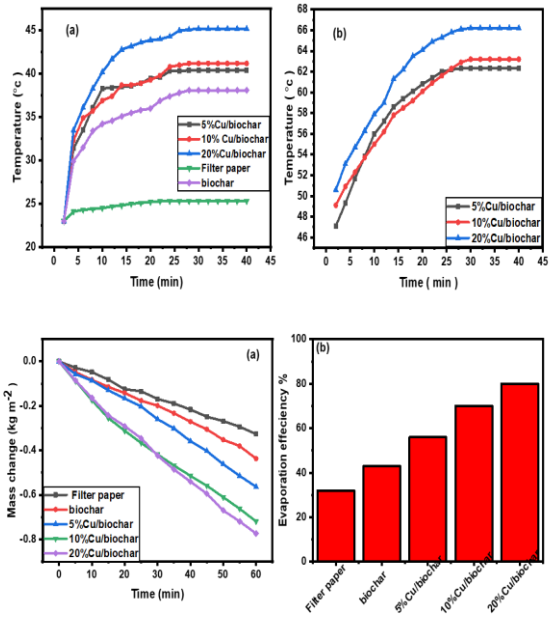

Fig.3 :(a) Water loss of all evaporators under 1sun illumination for 1h, (b) Evaporation efficiencies of as-synthesized samples.

3.3. Surface temperature

Additionally, a thermocouple and an IR imager were used to monitor the evaporators' surface temperatures as they were exposed to solar radiation. As shown in Fig. 4a. In the wet state, the top surface temperature of the (5% Cu/biochar, 10% Cu/biochar, and 20% Cu/biochar) solar absorbers quickly increased from room temperature to 40.4, 41.2, and 45.2 ℃, respectively. Due to the greatest solar absorption of both plasmonic metals and biochar evaporators, the surface temperature of 20% Cu/biochar is the highest among all the absorbers, demonstrating a superior photocatalytic efficiency. Additionally, filter paper has the lowest temperature change of any material (only 26.0 °C), demonstrating that there is no thermal evaporation rate. Additionally, Fig. 4b illustrated that these evaporators' surfaces' infrared thermal images in the dry state fast increased from room temperature to approximately 35.1, 41.1, 62.3, 63.5, and 66.4 °C in ten minutes and the entire hour of radiation was administered. The aqueous surface feature and mesoporous structure of the biochar influence the surface temperature of the evaporators in the liquid state (Fig. 4a), which is massively minimized but remains higher than the temperature of the bulk water. As can be seen in Fig. 4, the fact that the SSG surface is significantly warmer than the bulk water suggests that the insulator PU foam was successful in concentrating heat at the absorber surface and minimizing heat exchange into the bulk of solution.

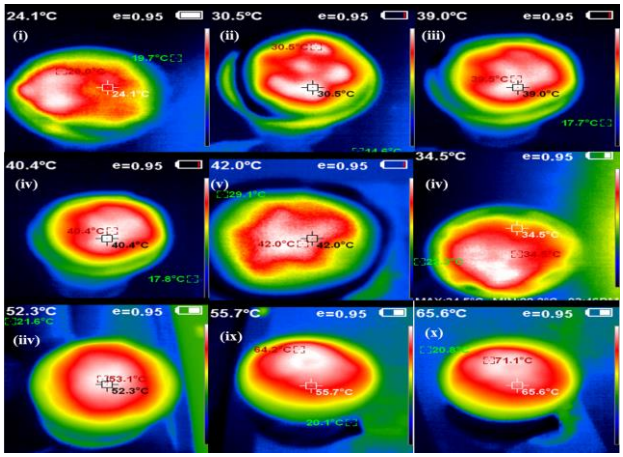

Fig.4: (a) Temperature- time curve in wet, (b) Temperature- time curve in dry, IR thermal images of (i) 1- **Air- laid paper**, (ii, iv) **biochar**, (iii, iiv) **5% Cu/biochar**, (iv, ix) **10% Cu/biochar** and (v, x) **20% Cu/biochar** in the wet and dry state under 1sun illumination for 1h, respectively.

3.4. Biochar salt-resistant and reusability effect

Additionally, under one sun illumination, ten continuous evaporation processes for saline water (20% NaCl) and DI water were carried out to verify the steady effectiveness of Cu/biochar system in SSG efficiency. Fig. 5 showed that the evaporation rate for both saline water and water did not decrease over cycles. Additionally, due to the biochar's salt rejection property, there was no saline accumulation on the evaporator surface after a continuous 10 hours (Fig. 5a). Due to the adhesive force between the glass wall and the salt crystals, cotton threads and salt crystallization both increased at the same time and attached to the container's outside enclosure wall [29]. After

the experiments, the evaporator's chemical stability was tested, and the outcomes demonstrated how our material exhibits higher chemical consistency thanks to SSG efficiency, according to the Figure.5b Additionally, the membrane's SSG was carried out in salt water with varying concentrations of NaCl (3%, 7%, 10%, and 20%). It was noted that the absorber showed a comparable rate of evaporation ratios in DI water and brine, demonstrating Cu/biochar membrane's excellent salt rejection performance even at high salinity water. Additionally, SSG tests were conducted on a variety of saline waters under one sun's irradiation, and the outcomes revealed that the evaporator had a steady SSG efficiency of around 0.774 kg m^{-2} h^{-1}.

To support a potential application of Cu/biochar, the SSG tests for synthetic saltwater (solution of K^+, Mg^{2+}, Na^+, and Ca^{2+}) were utilized as well. ICP measured the concentration of ions in the brine and condensed water during the 60-minute desalination process, which was carried out under one sun's illumination. According to the World Health Organization (WHO) that defined the standard values for drinkable water, it was shown that the concentration of primary ions in DI water is dramatically lowered to low levels. This suggests the membrane has an excellent capacity for purification Fig. 5c.

Additionally, dye-contaminated seawater was used for the SSG studies, which involved one solar exposure. The content of dyes was then measured after the evaporation performance. According to results, the increasing percentage of 20% Cu/biochar composite evaporation in the SSG of polluted seawater is evidence that the contaminants were totally eliminated from the water vapor. The SSG was carried out on acidic and alkaline water, and by using pH paper, the accumulated water's pH was calculated as illustrated in Figure.5d. To further demonstrate the membrane's capacity for purifying polluted seawater. The graph showed that the pH value of the evaporated water was 7, demonstrating the 20% Cu/biochar membrane's resistance to acid and alkali medium. Additionally, Fig.5e,f demonstrated that the water was purified after evaporation since the water vapour acquired a resistivity (131.7 K); which contrasted with the water's low resistance value before evaporation (5.4 K).

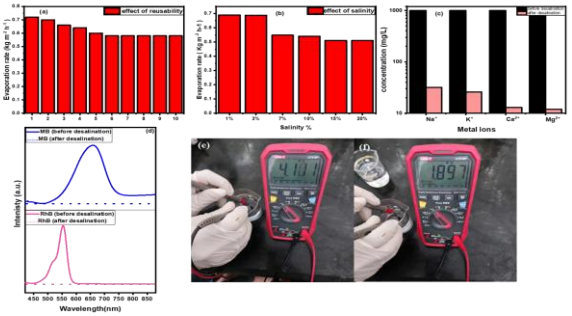

Fig.5: (a) Recyclability test of the 20%Cu/biochar membrane during continuous 10 cycles of SSG performance (20% NaCl), (b) Evaporation rate of membrane 20%Cu/biochar for different saline water under one sun illumination for 1h, (c) metal ions concentration, (d) UV-vis spectra of contaminated dyes, and Ohmic resistances of (e) contaminated and (f) condensed water.

3.5. Outdoor Solar desalination

Solar desalination was carried out for 9 hours under the real sun to assess the significant potential of 20% Cu/biochar for large-scale freshwater production. A power meter was used to measure the change in weight, interfacial temperature, and solar light intensity every hour. Fig. 6a illustrates a picture of the solar evaporation process during sunshine irradiation. As indicated in Figure, the sun's highest intensity of 765 W/m^2 (1 sun) was observed around 1:00 p.m., with intensity values of 649 W/m^2. Also, the rate of evaporating seawater was kept constant within 0.326 kg m^{-2} h^{-1} and 0.77 kg m^{-2} h^{-1} (Fig. 6b), with an average rate approaching 5.404 kg m^{-2} for 9 hours.

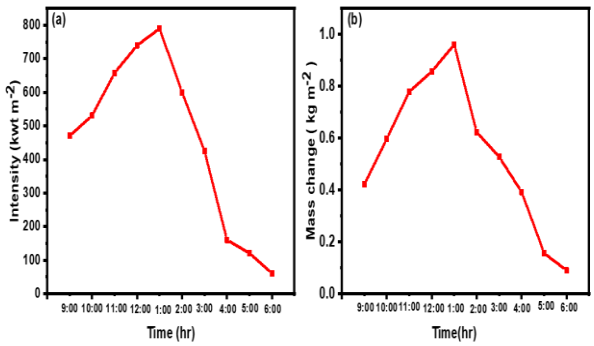

Fig.6: (a) Sun intensity of 20% Cu/biochar surface from 9:00 am to 5:00 pm, (b) Sun intensity and evaporation rate of 20% Cu/biochar from 9:00 am to 5:00 pm.

Conclusion

Finally, we demonstrated the construction of a highly efficient solar desalination and wastewater purification system that depends on plasmonic biochar. The Cu/biochar bilayer system as it was synthesized demonstrated great chemical stability, low thermal conductivity, excellent light-harvesting and macropore structures which made it a promising SSG technique. Cu/biochar, a photothermal material, has an energy conversion efficiency of up to 0.77% when exposed to solar radiation, and a high evaporation rate of 0.657 kg m^{-2} h^{-1} has been achieved. The absorber can combine effective water transmission with high salinity resistant due to coordinated action of nanopores in biochar construction. Additionally, because of the numerous functional groups in the biochar construction, the absorber displayed consistent absorption with nearly little salt accumulation for ten hours of continuous evaporation below one sunlight irradiation. Additionally, even in highly salinized water (20 wt %), the Cu/biochar demonstrated a clear ability to reject salt, pointing to the possibility of long-term photothermal transition for desalination processes This research may offer a fresh method for developing photothermal materials with greater salt-resistance and high efficiency for solar steam.

4. References

1. Karagiannis, I.C. and P.G. Soldatos, Water desalination cost literature: review and assessment. Desalination, 2008. **223**(1-3): p. 448-456.
2. Ramalingam, K., et al., Self-Sustained Visible-Light-Driven Electrochemical Redox Desalination. ACS Applied Materials & Interfaces, 2020. **12**(29): p. 32788-32796.
3. Cohen-Tanugi, D. and J.C. Grossman, Water desalination across nanoporous graphene. Nano Letters, 2012. **12**(7): p. 3602-3608.
4. Ni, G., et al., Steam generation under one sun enabled by a floating structure with *t*hermal concentration. Nature Energy, 2016. **1**(9): p. 16126.
5. Zhou, L., et al., *3D* self-assembly of aluminium nanoparticles for plasmon-enhanced solar desalination. Nature photonics, 2016. **10**(6): p. 393-398.
6. Sharon, H. and K.S. Reddy, A review of solar energy driven desalination technologies. Renewable and Sustainable Energy Reviews, 2015. **41**: p. 1080-1118.
7. Liu, K.-K., et al., Wood-Graphene Oxide Composite for Highly Efficient Solar Steam Generation and Desalination. ACS Applied Materials & Interfaces, 2017. **9**(8): p. 7675-7681.
8. Liu, Y., et al., A bioinspired, reusable, paper-based system for high-performance large-scale evaporation. Advanced Materials, 2015. **27**(17): p. 2768-2774.
9. Bae, K., et al., Flexible thin-film black gold membranes with ultrabroadband plasmonic nanofocusing for efficient solar vapour generation. Nature Communications, 2015. **6**: p. 10103.
10. Jonhson, W., et al., Fabrication of 3D-Printed Ceramic Structures for Portable Solar Desalination Devices. ACS Applied Materials & Interfaces, 2021. **13**(19): p. 23220-23229.
11. Wang, J., et al., High-Performance Photothermal Conversion of Narrow-Bandgap Ti2 O3 Nanoparticles. Advanced Materials, 2017. **29**(3).
12. Ding, D., et al., Non-stoichiometric MoO3-x quantum dots as a light-harvesting material for interfacial water evaporation. Chemical Communications, 2017. **53**(50): p. 6744-6747.
13. Khajevand, M., S. Azizian, and R. Boukherroub, Naturally abundant green moss for highly efficient solar thermal generation of clean water. ACS Applied Materials & Interfaces, 2021. **13**(27): p. 31680-31690.
14. Guo, Y., et al., Tailoring surface wetting states for ultrafast solar-driven water evaporation. Energy & Environmental Science, 2020. **13**(7): p. 2087-2095.
15. Li, W., et al., Portable Low-Pressure Solar Steaming-Collection Unisystem with Polypyrrole Origamis. Advanced Materials, 2019. **31**(29): p. e1900720.
16. He, W., et al., Structure development of carbon-based solar-driven water evaporation systems. Science Bulletin, 2021. **66**(14): p. 1472-1483.

17. Abo El-Yazeed, W.S., et al., Facile fabrication of bimetallic Fe-Mg MOF for the synthesis of xanthenes and removal of heavy metal ions. RSC advances, 2020. **10**(16): p. 9693-9703.
18. Fang, J., et al., Hierarchical porous carbonized lotus seedpods for highly efficient solar steam generation. Chemistry of Materials, 2018. **30**(18): p. 6217-6221.
19. Kuang, Y., et al., A High-Performance Self-Regenerating Solar Evaporator for Continuous Water Desalination. Advanced Materials, 2019 **31**(23): p. e1900498.
20. Li, W., et al., Porous wood-carbonized solar steam evaporator. Wood science and technology, 2021. **55**(3): p. 625-637.
21. Rawat, J., J. Saxena, and P. Sanwal, Biochar: A sustainable approach for improving plant growth and soil properties, in Biochar An Imperative Amendment for Soil and the Environment, V. Abrol and P. Sharma, Editors. 2019, IntechOpen.
22. Mohammadi, A., et al., A critical review on advancement and challenges of biochar application in paddy fields: environmental and life cycle cost analysis. Processes, 2020. **8**(10): p. 1275.
23. Li, H., et al., Mechanisms of metal sorption by biochars: Biochar characteristics and modifications. Chemosphere, 2017. **178**: p. 466-478.
24. Zhu, Y., et al., Removal of EDTA-Cu(II) from Water Using Synergistic Fenton Reaction-Assisted Adsorption by Nanomanganese Oxide-Modified Biochar: Performance and Mechanistic Analysis. ACS ES&T Water, 2021. **1**(5): p. 1302-1312.
25. Kawamura, G., et al., Production of Oxidation-Resistant Cu-Based Nanoparticles by Wire Explosion. Scientific Reports, 2015. **5**: p. 18333.
26. Dong, Y., et al., Synthesis and characterization of pure copper nanostructures using wood inherent architecture as a natural template. Nanoscale research letters, 2018. **13**(1): p. 119.
27. He, R., et al., Activated biochar with iron-loading and its application in removing Cr (VI) from aqueous solution. Colloids and Surfaces A: Physicochemical and Engineering Aspects, 2019. **579**: p. 123642.
28. Cheng, F. and X. Li, Preparation and Application of Biochar-Based Catalysts for Biofuel Production. Catalysts, 2018. **8**(9): p. 346.
29. Li, J., et al., Migration Crystallization Device Based on Biomass Photothermal Materials for Efficient Salt-Rejection Solar Steam Generation. ACS Applied Energy Materials, 2020. **3**(3): p. 3024-3032.